energy of acoustic free oscillations will be in part transfered to the resonant modes of seismic free oscillations to amplify the latter amplitudes. This amplification should depend critically on how close the resonant frequencies are between the solid Earth and the atmosphere. The eigenfrequencies of acoustic modes are sensitive to the acoustic structure of the atmosphere (12), which varies annually (19). The above difference between $_0S_{29}$ and other modes suggests that this annual variation of the acoustic structure more precisely tunes the resonant frequencies of acoustic modes to those of seismic modes in the summer of the Northern Hemisphere. We may alternatively attribute the annual variation of the oscillations to the variation of the source height, to which the excitation of coupled modes is sensitive. Thus, the observed phenomena are best explained by the atmospheric excitation hypothesis, although other possibilities, such as disturbances of oceanic origin, cannot be ruled out.

The phenomenon of the background free oscillations represents the hum of the solid Earth, which we found to be resonant with the hum of the atmosphere through the two frequency windows. The excitation source of the hum may be at lowest part of the convective zone of the troposphere, so that it is also responsible for the hum of the atmosphere. The hum in the resonant windows is louder and shows a greater annual variation. The phenomenon can be understood only if the two systems of the solid Earth and atmosphere are viewed as a coupled system.

References and Notes
1. K. Nawa et al., Earth Planet. Space 50, 3 (1998).
2. N. Suda, K. Nawa, Y. Fukao, Science 279, 2089 (1998).
3. T. Tanimoto, J. Um, K. Nishida, N. Kobayashi, Geophys. Res. Lett. 25, 1553 (1998).
4. N. Kobayashi and K. Nishida, Nature 395, 357 (1998).
5. K. Nishida and N. Kobayashi, J. Geophys. Res. 104, 28741 (1999).
6. N. Kobayashi and K. Nishida, J. Phys. Condens. Matter 10, 11557 (1998).
7. S. W. Smith, Eos 67, 213 (1986).
8. G. Roult and J. P. Montagner, Ann. Geofis. 37, 1054 (1994).
9. The 17 IRIS stations we analyzed were AAK (Ala Archa, Kyrgyzstan), BFO (Black Forest, Germany), COL (College Outpost, AK, USA), COR (Corvallis, OR, USA), CTAO (Charters Towers, Australia), ENH (Enshi, China), ESK (Eskdalemuir, Scotland), HIA (Hailar, China), KMI (Kunming, China), LSA (Lhasa, China), MAJO (Matsushiro, Japan), MDJ (Mudanjiang, China), PFO (Pinon Flat, CA, USA), SSE (Shanghai, China), SUR (Sutherland, Republic of South Africa), TLY (Talaya, Russia), and WMQ (Urumqi, China). The eight GEOSCOPE stations were CAN (Mount Stromlo, Canberra, Australia), HYB (Hyderabad, India), INU (Inuyama, Japan), KIP (Kipapa, HI, USA), NOUC (Port Laguerra, Nouvelle Caledonia), SCZ (Santa Cruz, CA, USA), TAM (Tamanrasset, Algeria), and WUS (Wushi, China).
10. A. M. Dziewonski and D. L. Anderson, Phys. Earth Planet. Inter. 25, 297 (1981).
11. D. C. Agnew and J. Berger, J. Geophys. Res. 83, 5420 (1978).
12. S. Watada, thesis, California Institute of Technology, Pasadena, CA (1995).
13. P. Lognonné, E. Clévédé, H. Kanamori, Geophys. J. Int. 135, 388 (1998);
14. P. Lognonné, B. Mosser, F. A. Dahlen, Icarus 110, 186 (1994).
15. H. Kanamori and J. Mori, Geophys. Res. Lett. 19, 721 (1992).
16. R. Widmer and W. Zürn, Geophys. Res. Lett. 19, 765 (1992).
17. H. Jacobowitz et al., J. Geophys. Res. 89, 4997 (1984).
18. R. Kandel et al., Bull. Am. Meteorol. Soc. 79, 765 (1998).
19. E. L. Fleming, S. Chandra, J. J. Barnett, M. Corney, Adv. Space Res. 10, 11 (1990).
20. We are grateful to a number of people who were associated with IRIS and GEOSCOPE. We thank N. Suda, K. Nawa, K. Nakajima, and S. Watada for comments on this paper.

11 November 1999; accepted 8 February 2000

Simulation of Early 20th Century Global Warming

Thomas L. Delworth* and Thomas R. Knutson

The observed global warming of the past century occurred primarily in two distinct 20-year periods, from 1925 to 1944 and from 1978 to the present. Although the latter warming is often attributed to a human-induced increase of greenhouse gases, causes of the earlier warming are less clear because this period precedes the time of strongest increases in human-induced greenhouse gas (radiative) forcing. Results from a set of six integrations of a coupled ocean-atmosphere climate model suggest that the warming of the early 20th century could have resulted from a combination of human-induced radiative forcing and an unusually large realization of internal multidecadal variability of the coupled ocean-atmosphere system. This conclusion is dependent on the model's climate sensitivity, internal variability, and the specification of the time-varying human-induced radiative forcing.

Confidence in the ability of climate models to make credible projections of future climate change is influenced by their ability to reproduce the observed climate variations of the 20th century, including the global warmings in both the early and latter parts of the century (1). Several climate models accurately simulate the global warming of the late 20th century when the radiative effects of increasing levels of human-induced greenhouse gases (GHGs) and sulfate aerosols are taken into account (2–4). However, the warming in the early part of the century has not been well simulated using these two climate forcings alone. Factors which could contribute to the early 20th century warming include increasing GHG concentrations, changing solar and volcanic activity (4–6), and internal variability of the coupled ocean-atmosphere system. The relative importance of each of these factors is not well known.

Here, we examine results from a set of five integrations of a coupled ocean-atmosphere model forced with estimates of the time-varying concentrations of GHGs and sulfate aerosols over the period 1865 to the present, along with a sixth (control) integration with constant levels of greenhouse gases and no sulfate aerosols. In one of the five GHG-plus-sulfate integrations, the time se-

ries of global mean surface air temperature provides a remarkable match to the observed record, including the global warmings of both the early (1925–1944) and latter (1978 to the present) parts of the century. Further, the simulated spatial pattern of warming in the early 20th century is broadly similar to the observed pattern of warming. Thus, we demonstrate that an early 20th century warming, with a spatial and temporal structure similar to the observational record, can arise from a combination of internal variability of the coupled ocean-atmosphere system and human-induced radiative forcing from GHG and sulfate aerosols. These results suggest a possible mechanism for the observed early 20th century warming.

The coupled ocean-atmosphere model that was used, developed at the GFDL, is higher in spatial resolution than an earlier version used in many previous studies of climate variability and change (7, 8), but it employs similar physics. The coupled model is global in domain and consists of general circulation models of the atmosphere (R30 resolution, corresponding to 3.75° longitude by 2.25° latitude, with 14 vertical levels) and ocean (1.875° longitude by 2.25° latitude, with 18 vertical levels). The model atmosphere and ocean communicate through fluxes of heat, water, and momentum at the air-sea interface. Flux adjustments are used to facilitate the simulation of a realistic mean state. A thermodynamic sea-ice model is used over oceanic regions, with ice movement determined by ocean currents.

Geophysical Fluid Dynamics Laboratory (GFDL)/National Oceanic and Atmospheric Administration, Princeton, NJ 08542, USA.

*To whom correspondence should be addressed. E-mail: td@gfdl.gov

The first integration is a 1000-year control case, with no year-to-year variations in external radiative forcing. After a small initial climate drift over the first 100 years, the coupled model is very stable for the remaining 900 years of the integration. In the other five integrations, an estimate of the observed time-varying concentrations of GHGs plus sulfate aerosols (9–11) is used to force the model over the period 1865–2000. The radiative perturbations associated with sulfate aerosols are modeled as prescribed changes in the surface albedo. The latter five integrations are identical in experimental design, with the exception of the initial conditions, which were selected from widely separated times in the control integration after the first 100 years. These integrations have previously been used to assess regional trends in observed surface temperature over the latter half of the 20th century (12).

Time series of annual mean, global mean surface temperature are constructed from both observations (13) and the model integrations using surface air temperature over land and sea-surface temperature (SST) over the ocean. The surface temperature time series from the five GHG-plus-sulfate integrations (Fig. 1A) show an increase over the last century, which is broadly consistent with the observations. The individual runs, denoted as experiments 1 through 5, form a spread around the observations, indicating the internal variability inherent in the model.

One of the integrations (experiment 3, shown in Fig. 1B) shows a remarkable similarity to the observed record, including the amplitude and timing of the warming in the early 20th century. Because the model includes no forcing from interdecadal variations of volcanic emissions or solar irradiance, this suggests that the observed early 20th century warming could have resulted from a combination of human-induced increases of atmospheric GHGs and sulfate aerosols, along with internal variability of the ocean-atmosphere system.

Given that a combination of internal variability and GHG and sulfate aerosol radiative forcing is able to produce a simulated early 20th century warming similar to that of the observed record, we can assess how likely such an occurrence is in the model. We first note that over the period 1910–1944, the linear trend in observed temperature is 0.53 K per 35 years, whereas the trend in the five-member ensemble mean is 0.21 K per 35 years; the difference between the two is 0.32 K per 35 years. We wish to evaluate the likelihood that the trend from a single realization of this model (such as experiment 3) would exceed the ensemble mean by 0.32 K per 35 years (as is the case for the observations). Using information from the long control integration (14), we estimate that such a

difference between a single realization and an independent five-member ensemble mean occurs approximately 4.8% of the time, demonstrating that although the 1910–1944 trend is a relatively rare occurrence for this model, it is still within the range of possibilities.

We now assess whether internal variability alone can account for the observed early 20th century warming, or if the radiative forcing from increasing concentrations of GHGs is also necessary. Over the period 1910–1944 (which encompasses the warming of the 1920s and 1930s), there is a linear trend of 0.53 K per 35 years in observed global mean temperature. If internal variability alone can explain this warming, comparable trends should exist in the control run. Linear trends were computed over all possible 35-year periods, using the last 900 years of the control run (i.e., years 101–135, 102–136, . . ., 966–1000). For each 35-year segment, the time-varying distribution of observed data over the period 1910–1944 was used to select the model locations for calculating the global mean. The maximum trend in any 35-year period of the control run is 0.50 K per 35 years. This suggests that internal model variability alone is unable to explain the observed early 20th century warming.

In terms of regional structure, the observed early 20th century warming shows a pronounced maximum at higher latitudes of the Northern Hemisphere (Fig. 2, top left). A similar warming at high latitudes of the Northern Hemisphere is also seen in experiment 3 (Fig. 2, top right), thereby lending credibility to the possibility that the model warming arises from physical processes similar to those important for the observed

warming. The four other GHG-plus-sulfate experiments show a range of variability in the early part of the record, illustrating the internal variability of the model. Interestingly, a warming at high latitudes of the Northern Hemisphere is seen in the late 1800s of experiment 1, illustrating that aspects of the warming seen in the 1920s and 1930s of experiment 3 occur at other times. Also notable is the pronounced high northern latitude cooling in the 1920s and 1930s that occurs in experiment 5. A more general warming occurs over the last several decades in all the experiments and in the observations, suggesting a robust forced response of the climate system during this period to increasing concentrations of GHGs (2–4).

The spatial pattern associated with the early 20th century warming is further evaluated by computing linear trends over the period 1910–1944 at each grid point for both the available observations and experiment 3 (Fig. 3). For the observations, the warming is largest in the Atlantic and North American regions. Although the ensemble mean trend (Fig. 3B) shows a more spatially homogeneous pattern of warming (as expected from ensemble averaging), the pattern from experiment 3 (Fig. 3C) bears a considerable resemblance to the observed trend. There are relatively large regional differences, however, in the northwestern North Atlantic. We can evaluate the degree to which the observed local temperature trends are consistent with the local temperature trends of the ensemble mean, taking into account the internal variability of the model. Using a local t test, the gray shading in Fig. 3D denotes regions where the observed and simulated trends are consistent, whereas color shading denotes re-
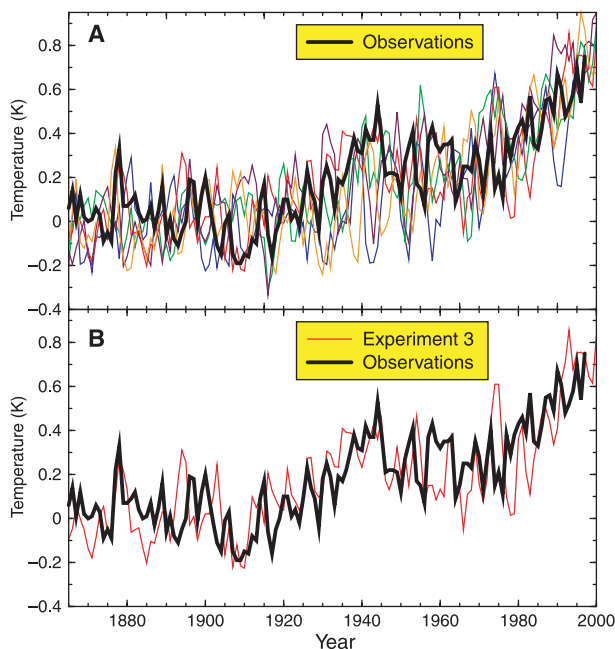

Fig. 1. (**A**) Time series of global mean surface temperature from the observations (heavy black line) and the five model experiments (various colored lines). Surface air temperature is used over land, while SST is used over the oceans. Units (in K) are expressed as deviations from the period 1880–1920. In constructing the global means for the model, the model output is sampled only for times and locations where observational data are available. (**B**) Same as (A), except that only one of the model results (experiment 3) is shown.

gions where the observed and simulated trends are significantly different at the $P = 0.10$ level according to the local t test (15). By this measure, the differences in the trends over the northwestern Atlantic are not statistically significant. However, the observed warming in the tropical and subtropical Atlantic is significantly underestimated by the model.

Additional characteristics of the simulated warming for which no comparable direct observations are available can also be evaluated. The ensemble mean model output was time-averaged over the period 1921–1944, and then subtracted from the 1921–1944 time-mean of experiment 3. These differences denote the characteristics of the internal vari-

ability associated with the 1920s and 1930s warming in experiment 3. The warming was largest in the high-latitude North Atlantic, and the Nordic and Barents Seas. The upper oceans in these regions were characterized by increased temperature, salinity, and density, along with reduced sea-ice cover which extended into the Arctic. The reduction in sea-
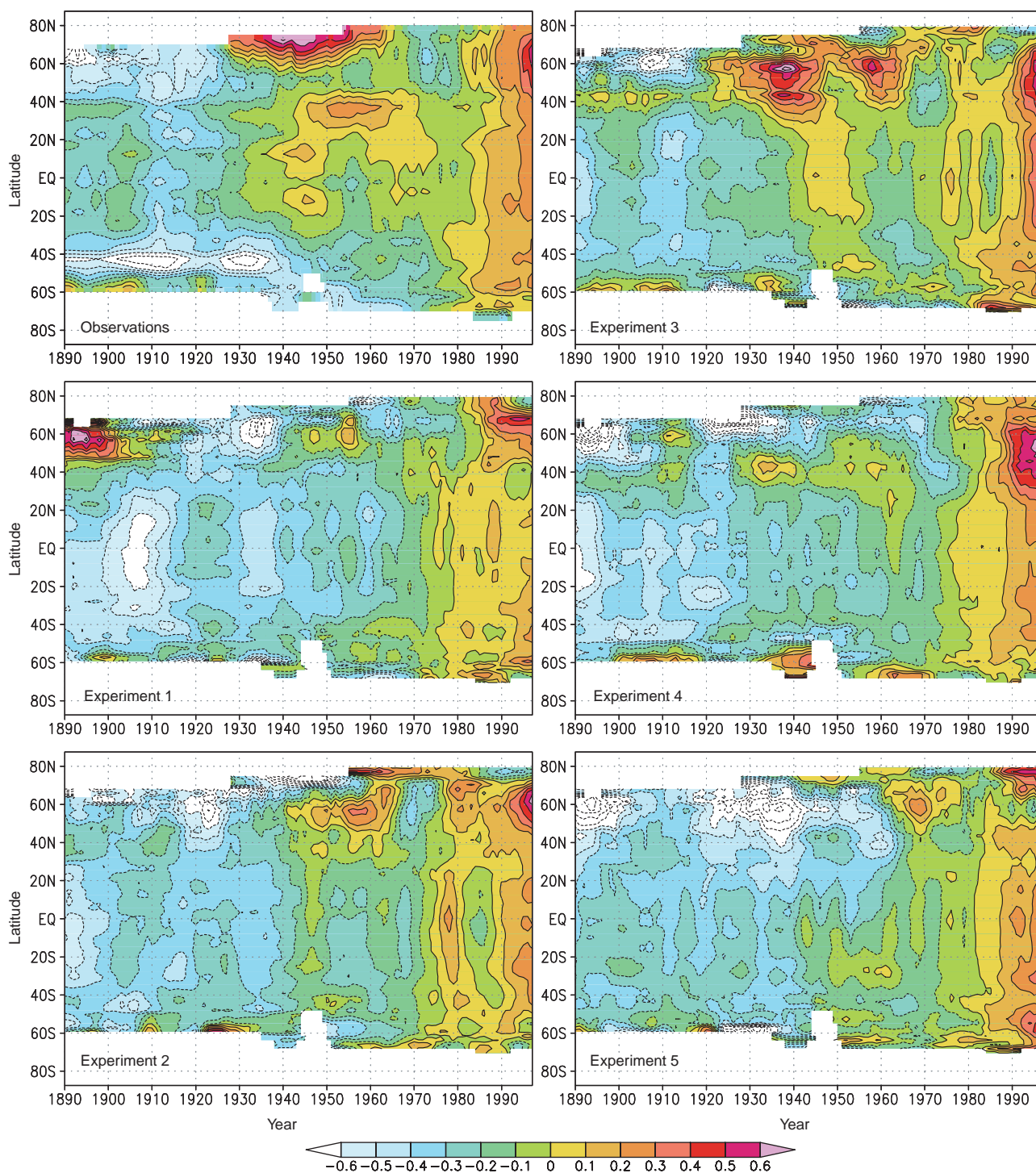

Fig. 2. Zonal mean anomalies of surface temperature (in K) for the observations (upper left panel) and the five model experiments. Prior to plotting, all values were subjected to a 10-year low-pass filter; values are plotted at the ending year of the 10-year period. For the model output, only times and locations for which there were observational data were used in the calculations. Anomalies are relative to the 1961–1990 climatology.

ice cover reduced near-surface albedos and appeared to play a role in increasing the radiative forcing of the surface.

The increased upper ocean density in the high latitudes of the North Atlantic is associated with an enhanced thermohaline circulation (THC) (22% larger than the ensemble mean of 14.3 Sv over the period 1921–1944; 1 Sv = 10^6 m^3 s^{-1}). The enhanced THC appears to play a role in the warming through an increased meridional transport of heat and an increased ocean-to-atmosphere heat flux. Additional analyses suggest that the enhanced THC is at least partially attributable to a persistent positive phase of the model-simulated North Atlantic Oscillation (NAO) from approximately 1910 to 1950, peaking in the late 1920s. This aspect of the simulated NAO resembles the observed NAO (16) and associated wind changes (17). Many of the above features are seen in typical realizations of multidecadal climate variations linking the Arctic and North Atlantic in the control simulation. They also resemble previously documented (18) variability in a lower resolution version of this coupled model, as well as available results from the instrumental record (19, 20) and proxy reconstructions (21) of the climate record.

Several important caveats must be considered when interpreting the results of this study. First, the model has a cold bias in the

climate of the North Atlantic, leading to more sea ice than is observed in that region. Second, the simulated standard deviation of SST anomalies is larger in some parts of the North Atlantic than has been observed. The combination of these factors may lead, through ice-albedo feedback, to multidecadal variability which is larger than that of the real climate system, thereby influencing the interpretation of the above results. To shed light on this, analyses similar to those above (14) were conducted on an additional 500-year control integration, using a version of the model in which the sea-ice bias in the North Atlantic was reduced through an altered initialization procedure. In ~2.3% of the cases for that integration, the difference between a single 35-year segment and the mean of five other 35-year segments exceeded 0.32, thereby indicating a reduced likelihood (2.3%) of a single integration capturing the early 20th century warming compared with the primary model employed for this study (4.8%).

From a different perspective, a recent study (22) concluded that the high-latitude variability in a model can be rather dependent on the sea-ice model used. Unfortunately, the shortness of the instrumental record, particularly at high latitudes, makes the evaluation of model variability on multidecadal time scales extremely difficult. It is, therefore, of paramount impor-

tance to further develop and augment the instrumental and proxy records of climate variability on decadal to centennial time scales, as well as to improve modeling capabilities.

The results of this study depend on the climate sensitivity of the model, defined as the equilibrium temperature response to a doubling of atmospheric CO_2. If the climate sensitivity were smaller, then one would need either larger internal variability or additional radiative forcings to capture the early 20th century warming. The climate sensitivity of this model is approximately 3.4 K, which is in the upper half of the 1.5 to 4.5 K range cited by the Intergovernmental Panel on Climate Change (23). In addition, the ensemble mean warming simulated by the GFDL model over the period 1945–1995 is larger than some other coupled models (24, 25).

A recent comprehensive study (4) of the simulated climate of the 20th century suggested that there could be some contribution of solar forcing to the warming in the early part of the 20th century, but its quantification is problematic. Additional work (26) showed that detecting a solar influence in the early 20th century depends on which solar forcing reconstruction is used. Because the integrations used here do not contain interdecadal variations of volcanic or solar forcing, we can make no assessment of the potential contri-
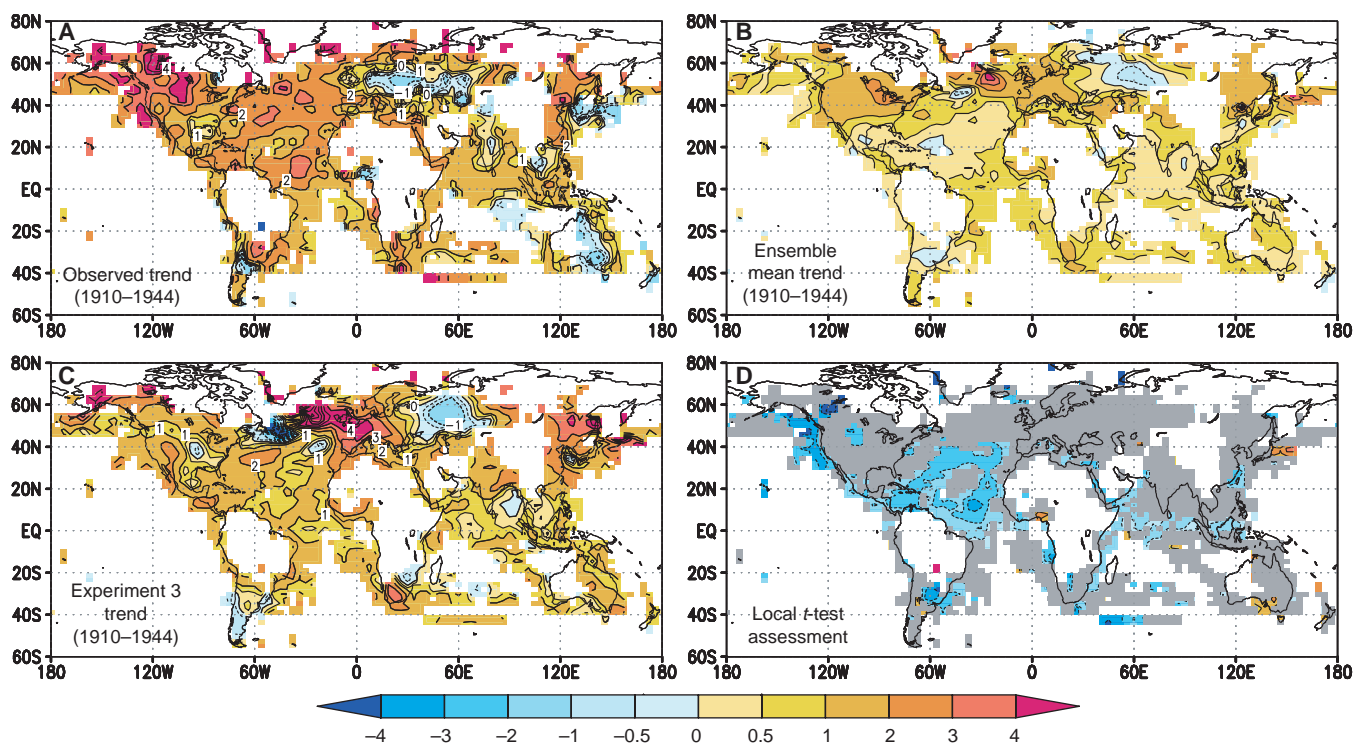

Fig. 3. (A) Linear trends of surface temperature (expressed as K per 100 years) over the period 1910–1944 for the available observations; (B) Same as (A) except for the five-member ensemble mean of the coupled model simulations; (C) Same as (B) but for experiment 3 only; (D) Result of a local *t* test comparing the ensemble mean trend and the observed trend over the period 1910–1944. Gray shading denotes regions where the ensemble mean trend is consistent with the observed trend when one takes into account the internal variability of the coupled system as computed from the long control integration. Color shaded (nongray) regions denote an inconsistency [i.e., that the ensemble mean trend and observed trend are significantly different at the $P = 0.10$ level according to a two-sided two-sample *t* test (15)]; this occurs for 27% of the total area for which there is sufficient observational data. The colored shading has the same units as (A).

bution of those forcings to the warming of the early 20th century. However, these results do suggest that attempts to extract the response to solar forcing by correlating estimates of solar forcing with the observed temperature record can be misleading. Although some estimates of solar forcing do correlate with the observed record, they also correlate well with our experiment 3.

If the simulated variability and model response to radiative forcing are realistic, our results demonstrate that the combination of GHG forcing, sulfate aerosols, and internal variability could have produced the early 20th century warming, although to do so would take an unusually large realization of internal variability. A more likely scenario for interpretation of the observed warming of the early 20th century might be a smaller (and therefore more likely) realization of internal variability coupled with additional external radiative forcings. Additional experiments with solar and volcanic forcing, as well as with improved estimates of the direct and indirect effects of sulfate aerosols, will help to further constrain the causes of the early 20th century warming. Our results demonstrate the fundamental need to perform ensembles of climate simulations in order to better delineate the uncertainties of climate change simulations associated with internal variability of the coupled ocean-atmosphere system.

References and Notes

1. P. D. Jones, M. New, D. E. Parker, S. Martin, I. G. Rigor, *Rev. Geophys.* **37**, 173 (1999).
2. B. D. Santer *et al.*, *Nature* **382**, 39 (1996).
3. G. C. Hegerl *et al.*, *Clim. Dyn.* **13**, 613 (1997).
4. S. F. B. Tett, P. A. Stott, M. R. Allen, W. J. Ingram, J. F. B. Mitchell, *Nature* **399**, 569 (1999).
5. T. J. Crowley and K.-Y. Kim, *Geophys. Res. Lett.* **26**, 1901 (1999).
6. M. Free and A. Robock, *J. Geophys. Res.* **104**, 19057 (1999).
7. S. Manabe and R. J. Stouffer, *J. Clim.* **7**, 5 (1994).
8. _____, M. J. Spelman, K. Bryan, *J. Clim.* **4**, 785 (1991).
9. J. F. B. Mitchell, T. C. Johns, J. M. Gregory, S. F. B. Tett, *Nature* **376**, 501 (1995).
10. J. F. B. Mitchell, R. A. Davis, W. J. Ingram, C. A. Senior, *J. Clim.* **8**, 2364 (1995).
11. J. M. Haywood, R. J. Stouffer, R. T. Wetherald, S. Manabe, V. Ramaswamy, *Geophys. Res. Lett.* **24**, 1335 (1997).
12. T. R. Knutson, T. L. Delworth, K. W. Dixon, R. J. Stouffer, *J. Geophys. Res.* **104**, 30981 (1999).
13. D. E. Parker, P. D. Jones, A. Bevan, C. K. Folland, *J. Geophys. Res.* **99**, 14373 (1994).
14. For fully overlapping 35-year periods from model years 101 to 1000 (i.e., years 101–135, 102–136, . . ., 966–1000), we projected the model output onto the same grid used for the observations. The model output was then sampled according to the temporal and spatial distribution of observed data over the period 1910–1944 to form global mean, annual mean time series from which linear trends are calculated. This yielded a set of 866 trends of duration 35 years. We then randomly selected six samples of nonoverlapping 35-year periods and computed the difference between the trend in the first sample and the mean of the trends for the other five samples. This process was repeated one million times to produce a distribution of differences between a single trend (realization) and five-member ensemble means. Using this
distribution, we then evaluated how likely the difference is between the trend corresponding to the observations (viewed as a single realization) and the five-member ensemble mean trend. Differences equal to or exceeding 0.32 K/year (the difference between the observed trend and the ensemble mean model trend) occurred in 4.8% of the cases, indicating the likelihood that the observed trend is consistent with the model ensemble. This assessment depends on the assumption that internal variability in the five transient runs is similar to that in the control run.
15. The ensemble mean trend from the five GHG-plus-sulfate experiments ($n = 5$) was compared with the observed trend ($n = 1$) at each grid point (with sufficient temporal coverage), using a local two-sided two-sample t test. The population variance for the t test was estimated from 35-year trends as simulated in the 900-year control integration. For the t test, we assumed 25 degrees of freedom, based on the number of nonoverlapping 35-year chunks in the control integration. Assuming only 20 degrees of freedom, the percent area rejecting the null hypothesis decreases only slightly (from 27 to 26%).
16. J. W. Hurrell, *Science* **269**, 676 (1995).
17. J. C. Rogers, *J. Clim. Appl. Meteorol.* **24**, 1303 (1985); C. Fu, H. F. Diaz, D. Dong, J. O. Fletcher, *Int. J. Climatol.* **19**, 581 (1999).
18. T. L. Delworth, S. Manabe, R. J. Stouffer, *Geophys. Res. Lett.* **24**, 257 (1997).
19. M. E. Schlesinger and N. Ramankutty, *Nature* **367**, 723 (1994).
20. M. E. Mann and J. Park, *J. Clim.* **9**, 2137 (1996).
21. _____, R. S. Bradley, *Nature* **378**, 266 (1995); T. L. Delworth and M. E. Mann, *Clim. Dyn.*, in press.
22. D. S. Battisti, C. M. Bitz, R. E. Moritz, *J. Clim.* **10**, 1909 (1997).
23. A. Kattenberg *et al.*, in *Climate Change 1995: The Science of Climate Change*, J. Houghton *et al.*, Eds. (Cambridge Univ. Press, Cambridge, 1996), pp. 285–357.
24. T. P. Barnett *et al.*, *Bull. Am. Meteorol. Soc.* **80**, 2631 (1999).
25. M. R. Allen, P. A. Stott, J. F. B. Mitchell, R. Schnur, T. L. Delworth, *Technical Report RAL-TR-1999-084* (Rutherford Appleton Laboratory, Chilton, Didcot, UK, 1999).
26. P. A. Stott, S. F. B. Tett, G. A. Jones, M. R. Allen, W. J. Ingram, J. F. B. Mitchell, *Clim. Dyn.*, in press.
27. We thank M. Allen, J. Anderson, A. Broccoli, K. Dixon, G. Hegerl, I. Held, P. Kushner, J. Mahlman, S. Manabe, and R. Stouffer for helpful contributions at various stages of the work.

6 October 1999; accepted 11 February 2000

Rapid Extinction of the Moas (Aves: Dinornithiformes): Model, Test, and Implications

R. N. Holdaway[1]* and C. Jacomb[2]

A Leslie matrix population model supported by carbon-14 dating of early occupation layers lacking moa remains suggests that human hunting and habitat destruction drove the 11 species of moa to extinction less than 100 years after Polynesian settlement of New Zealand. The rapid extinction contrasts with models that envisage several centuries of exploitation.

All 11 species of the large (20 to 250 kg) flightless birds known as moas (Aves: Dinornithiformes) survived until the arrival of Polynesian colonists in New Zealand (*1*). Abundant remains of moas in early archaeological sites show that the birds were major items of diet immediately after colonization (*2–5*). Indeed, the presence of moa remains was formerly used to characterize the earliest or "Archaic" period of human occupation in New Zealand [the "Moa-hunter" period (*3, 6*)]. Polynesian hunting and habitat destruction were responsible for the extinction of all species of moa some time before European contact began in the late 18th century (*1–4, 7*). Sites from the later, "Classic" Maori period lack evidence of moa exploitation. The Classic period is characterized by earthwork fortifications (the Maori term for which is *pa*) and occupation deposits indicating reliance on fish, shellfish, and plants for food.

Current interpretations of moa extinction implicitly or explicitly require a period of several hundred years of gradual population attrition by hunting and habitat loss: this is the orthodox model (*2, 3, 5*). The moa-hunting period has been estimated to have lasted some 600 years, peaking 650 to 700 years before the present (yr B.P.) and ending about 400 yr B.P. (*2, 3*). Anderson (*2*) estimated the duration of moa hunting from a radiocarbon chronology of moa hunting sites and from moa population parameters based on extant ratites and African bovids. It is difficult to estimate the time of moa extinction from a series of dates on moa bones and from moa hunting sites, because confidence intervals for calibrated ages are greater than those for conventional radiocarbon ages (*8*), and additional dates could be younger than the presently perceived limit.

Reassessment of some major archaeological sites has suggested that moas were becoming scarce by the end of the 14th century (*9, 10*). The earliest settlement sites date from the late 13th century (*11*), not the 10th or 11th century as previously thought (*5*). A later date for first settlement would imply that moa

[1]Palaecol Research, 167 Springs Road, Hornby, Christchurch 8004, New Zealand. [2]Canterbury Museum, Rolleston Avenue, Christchurch, New Zealand.

*To whom correspondence should be addressed. E-mail: piopio@netaccess.co.nz